Article

Journal of
Nanopharmaceutics and Drug Delivery
Vol. 2, 1–11, 2014
www.aspbs.com/jnd

Imaging of Guerin Carcinoma During Magnetic Nanotherapy

Valerii Orel[1,5,*], Thanos Mitrelias[2,3], Marina Tselepi[2,3], Tatyana Golovko[1], Oleh Dynnyk[4], Nikolay Nikolov[1,5], Andriy Romanov[1], Alexander Rykhalskiy[1], C. Crispin Barnes[2], Olga Yaroshenko[5], Irina Orel[1], Dmitriy Supruniuk[5], and Igor Shchepotin[1]

[1] *Head of Medical Physics and Bioengineering Research Laboratory, National Cancer Institute/33/43 Lomonosova Street, Kyiv 03022, Ukraine*
[2] *Cavendish Laboratory, University of Cambridge/JJ Thomson Avenue, Cambridge CB3 0HE, United Kingdom*
[3] *Cavendish NanoTherapeutics Ltd./CPC1 Capital Park, Fulbourn, Cambridge CB21 5XE, United Kingdom*
[4] *Bogomoletz Institute of Physiology/4 Bogomoletz Street, Kyiv, 01024, Ukraine*
[5] *National Technical University of Ukraine 'Kyiv Polytechnic Institute'/37 Prospect Peremogy, Kyiv, 03056, Ukraine*

We conducted a detailed imaging study of transplanted Guerin's carcinoma in rats during treatment with magnetic nanotherapy. We show that treatment with magneto-mechano-chemically synthesized magnetic nanocomplexes based on Fe_3O_4 nanoparticles conjugated with the antitumor agent doxorubicin and followed by irradiation with local electromagnetic irradiation resulted in a better outcome than treatment with conventional doxorubicin or treatment with magnetic nanocomplexes without electromagnetic irradiation. Analysis of magnetic resonance images obtained over time showed that the application of local electromagnetic irradiation did not alter the position of magnetic nanocomplexes in the tumor. B-mode sonography demonstrated that injection of magnetic nanocomplexes into the tumor and subsequent electromagnetic irradiation resulted in increased echogenicity throughout the tumor, which is characteristic of increased blood perfusion. Color Doppler ultrasound imaging showed that the largest decrease of tumor vessel area occurred after injection of magnetic nanocomplex and application of local electromagnetic irradiation. Elastography performed on a diagnostic ultrasound system showed that the injection of magnetic nanocomplexes in tumors increased Young's modulus for Guerin's carcinoma compared to tumors not treated with nanoparticles. These results suggest that a theranostics approach-combination MRI together with ultrasound elastography during treatment of tumor may provide a useful method to monitor the effectiveness treatment of cancer patients during magnetic nanotherapy.

KEYWORDS: *Tumor, Magnetic Nanotherapy, Digital Images, Magnetic Resonance Imaging, Ultrasound, Elastography.*

INTRODUCTION

Nanotechnology holds tremendous promise for the diagnostics and treatment of cancer. For example, nanotechnology applications may improve drug delivery, imaging contrast, and tumor hyperthermia compared with conventional cancer treatments.[1]

Magnetic nanocomplexes (MNC) containing iron oxide (magnetite) Fe_3O_4 have been used for both targeted magnetic drug delivery and induction of tumor hyperthermia. In targeted magnetic drug delivery, iron oxide containing nanoparticles are loaded with a therapeutic agent such as the antitumor anthracycline antibiotic doxorubicin (DOX). Application of a static magnetic field guides the iron oxide containing nanoparticles to a tumor and holds them there. In order to expose the particles to the highest possible traction force, magnetic drug targeting uses magnets with inhomogeneous fields. The goal of magnetic drug targeting is to concentrate the active ingredient specifically in the tumor region while at the same time minimizing the side effects of chemotherapy. In addition, tumor hyperthermia can be induced by heating the magnetic nanoparticles with a low and medium frequency external magnetic field (providing local hyperthermia), which weakens the tumor and increases the cytotoxic effects of chemotherapeutic

*Author to whom correspondence should be addressed.
Email: v-orel@voliacable.com
Received: 11 April 2014
Revised/Accepted: 3 August 2014

drugs. Thus, permanent magnetic gradient fields have been used for nanoparticle-mediated drug delivery, whereas a low-frequency alternating field is required for nanoparticle induced hyperthermia. The application of the alternating magnetic field generates heat via Brownian motion, Néel relaxation and/or due to magnetic hysteresis losses.[2]

A number of imaging technologies can be used to monitor tumor biology before and after nanotherapy. Such monitoring can provide direct evidence of the distribution and accumulation of nanoparticles in the tissue of interest and help fine-tune the condition and properties of the nanotherapy. Useful imaging technologies include nuclear medical imaging, magnetic resonance imaging (MRI), and ultrasound (US).

Nuclear medicine techniques can be used to estimate the effective (integrated/total) tumor perfusion. In our previous studies, using ^{99m}Tc-MIBI and ^{99m}Tc-pyrophosphate, we have shown in principle the possibility of increasing the accumulation of magnetic nanoparticles in a tumor by application of moderate radiofrequency hyperthermia and a static magnetic field.[3] In our previous study nuclear medicine techniques made it possible to estimate the percentage of drug accumulation in the tumor and the integral and local speed hemodynamic parameters. However, due to the low resolution of the gamma camera and the relatively small size of the tumor, it was not possible estimate the spatial distribution of the radiopharmaceutical in the tumor with tissue heterogeneity function.

MRI uses the fact that the tissues of the body contain a large amount of water, and, therefore, protons (nuclei ^{1}H) with magnetic spins that are aligned in a strong magnetic field.[4] In MRI imaging, superparamagnetic particles made of iron oxide can be used as contrast agents as they strongly influence T1 and T2 relaxation of water molecules near the metal. In other words, the rate of relaxation of excited water molecules near the metal is crucial for the image.[5] In general, MRI is an informative method for visualization of magnetic nanoparticles (Fe_3O_4), as well as a rough estimate of the heterogeneity of tissues.

Ultrasound imaging is a noninvasive medical technique in which reflected acoustic waves are used to produce an image of organs and other structures in the body. Ultrasound imaging is well suited to visualize textural heterogeneity of tumors. However, quantification methods are still imperfect. Elastography is a new noninvasive ultrasound technique which aims to exploit differences in tissue stiffness or elasticity.[6] Tumors are usually 5–28 times stiffer than the background of normal soft tissue; therefore, when a mechanical compression or vibration is applied, the tumor deforms to a lesser extent than the surrounding tissue. That is, the tension in tumors is less than in the surrounding tissue. Thus, the image deformation, under certain simplifying assumptions, can be represented as the spatial distribution of Young's modulus. The strain distribution can vary depending on the perfusion of biology fluid.[7]

Quantitative analysis is an important element of the correct interpretation of images, and quantitative image analysis has thus become an important tool for research in oncology. Image processing of nanoparticles is often based on nonlinear computer algorithms.[8]

In previous pilot studies we have shown that following the injection of the MNC into rats with Guerin carcinoma subjected to external electromagnetic radiation, the survival rates increased by 25% compared to the treatment with conventional doxorubicin alone.[9] However, MNC are also good candidates for contrast agents for MRI imaging of tumors. It is interesting to see what the effect of MNC accumulation in the tumor will be in the elasticity (Young modulus) of the tissues. If changes occur and those can be measured by ultrasound elastography, then one could envision a complete theranostics approach for our proposed magnetic nanotherapy: i.e., combination of diagnostic MRI together with elastography during administering magnetic nanotherapy. This approach could improve our ability to deliver individual tumor treatment. In this study, we present a detailed MRI and US imaging analysis of rats with transplanted Guerin's carcinoma treated with doxorubicin-containing MNC, in order to gain a better understanding of the way tumors react to this therapy.

MATERIALS AND METHODS

Experimental Animals and Tumor Transplantation

Female rats used in this study weighed 100 ± 15 g and were bred in the vivarium of the National Cancer Institute (Kiev, Ukraine). Guerin carcinoma transplantation was performed in accordance with established procedures. All animal procedures were carried out according to the rules of the Regional Committee for Animals and Medical Research Ethics of National Cancer Institute, Ukraine. Animals were divided into 5 groups: group 1—control (no treatment), group 2—treatment of DOX, group 3—electromagnetic irradiation (EI) + DOX treatment, group 4—treatment of MNC, group 5—treatment of MNC + EI.

Magnetic Nanocomplexes

MNC consisted of nanoparticles containing Fe_3O_4 (Sigma-Aldrich) and DOX (Pfizer, Italy), with diameters <50 nm. Synthesis of MNC was performed in a magneto-mechanical-reactor (National Cancer Institute, Ukraine). Mechanical processing was performed by vertical vibrations of the chamber at a frequency of 36 Hz and an amplitude of 9 mm for 5 min using mechanical energy of 20 W/g. Simultaneously, EI was applied for 5 minutes at 42 MHz by an induction coil with 40 W initial power and permanent magnets with magnetic field intensity 11 mT (in the centre). Mass concentration of DOX in MNC was 43%. MNC had saturation magnetic moment $m_s = 30.3$ emu/g and coercive force $H_c = 45.7$ Oe in an applied saturation magnetic field (H for m_s) $H_{ms} = 3000$ Oe. The electron spin g-factor (dimensionless magnetic moment) $= 2.7$.[10]

Treatment of Guerin's Carcinoma

Animal tumors were irradiated locally. Experimental animals were treated by DOX with a dose of 1.5 mg/kg and MNC with a dose of 3.5 mg/kg (DOX/Fe_3O_4 ratio was 1.5:2). Treatment was performed three times every 48 hours by intravenous infusion of DOX or MNC and EI from the 9th to the 13th day after tumor transplantation. Tumor size was measured by sliding calipers. Tumor volume before treatment was 0.82 ± 0.14 cm^3. Drugs were injected directly into the tumor. Tumor temperature during EI was measured in the tumor centre by the fiber-optic thermometer TM-4 (Radmir, Ukraine). Tumor temperature did not exceed 38.5–39.5 °C after 15 min EI. Preliminary research showed that 15 and 30 minutes of local EI on conventional Guerin carcinoma resulted in practically identical strengthening of DOX antineoplastic activity.[11] Thus, in order to maintain mild hyperthermia (below 40 °C), irradiation was performed for 15 minutes after administration of DOX or MNC. Electromagnetic radiation was produced by a prototype medical device "Magnetotherm" (Radmir, Ukraine) with spatially inhomogeneous electromagnetic field at a frequency of 40 MHz and an output power of 75 W.[12]

Magnetic Resonance Imaging

MRI was performed by MRI Signa Ovation (General Electric) with power induction 0.35 T. Studies were conducted on the backs of immobilized animals. Scanning was performed in neurovascular radio frequency coil, slice thickness 3 mm; synchronizing breathing was not used. MRI scanning involved the entire body. A tomogram was made in three orthogonal projections. For optimal cut layout was performed to obtain images in the coronal plane T2-WI, and T1-WI. Later in the study, protocol included axial scanning plane in T1 and T2-weighted images (WI) and sagittal plane in T2-WI.

Ultrasound Imaging

Tumor size and heterogeneity of tumor tissue were measured and monitored before and after therapeutic procedures using the ultrasound B-mode device SLE-901 (MEDELKOM, Lithuania) with a transducer frequency of 5 MHz. Color Doppler examination, elastography and dynamic viscosity were performed with the diagnostic ultrasound system "ULTIMA SE" (Radmir, Ukraine).[13]

Data Analysis and Digital Image Processing

The nonlinear kinetics of tumor volume growth were evaluated by the growth factor φ according to the autocatalytic equation

$$\frac{dx}{dt} = \varphi(x + x_0)(1 - x) \qquad (1)$$

where $x = (\Phi - \Phi_0)/(\Phi_\infty - \Phi_0)$ is the relative tumor growth by time t; $x_0 = \Phi_0/(\Phi_\infty - \Phi_0)$ is the relative tumor volume at the moment of time $t = 0$; Φ_0 and Φ_∞ is the initial and limiting tumor volume accordingly; Φ is the tumor volume at the moment of time t.[14]

The solution of Eq. (1) is

$$\Phi = \Phi_0 + \Phi_0 \cdot \frac{e^{\varphi(\Phi_\infty/(\Phi_\infty - \Phi_0))\cdot t} - 1}{1 + (\Phi_0/(\Phi_\infty - \Phi_0)) \cdot e^{\varphi(\Phi_\infty/(\Phi_\infty - \Phi_0))\cdot t}} \qquad (2)$$

The effect of EF and local IH on the nonlinear dynamics of the growth of animal tumors was evaluated with the braking ratio.

$$\kappa = \frac{\varphi_C}{\varphi_T} \qquad (3)$$

where φ_C is the growth factor for the control group of animals, φ_T is the growth factor for the treated group.

To quantify the changes in the spatial distribution of MNC in the tumors as seen by MRI on equivalent sections, we calculated the centre of mass of the particles conglomerates and the average radius between the centre and the particles.[15] The centre of mass was calculated from the binary image, where the pixels corresponding to the nanoparticles were assigned the value of one, and the rest a zero. Since the absolute value of the mean radius is of limited meaning, it was subsequently normalized to the size of the tumor in the image.

Textural analysis was performed to estimate changes in blood perfusion within tumor tissue after EI. The textural heterogeneity of the tumor in ultrasound images was evaluated based on the spatial autocorrelation coefficient Moran (r).[16]

Performance measurement of hemodynamics (perfusion) of the tumor as a result of color Doppler mapping was carried out by calculating the area of color patterns on ultrasound images (Sq). In this case, an important methodological feature of the study was the same scale flow velocity in different animals that make up the control group. Absolute parameters of blood flow in single tumor vessels were assessed using standard parameters: systole (S), diastole (D), resistance index (RI).

Elastography results were evaluated by the maximum value of Young's modulus (E_{max}) in the tumor, its average value (E_{av}), and the variance (σ_E^2). The probability density distribution of the Young's modulus ($p(E)$) was assessed on the basis of the Shannon entropy (Ω) parameter. Additionally, the unit "ULTIMA SE" provided an opportunity to quantify the strength of fabrics: average (η_{av}) value of viscosity.

Statistical Analysis

Statistical comparisons of data were performed using the Student's t-test when the data complied with conditions of normality and equal variance. The Kolmogorov-Smirnov method was used to test for normality. A significance criterion of $p < 0.05$, determined from two-tailed test, was used.

Table I. The growth kinetics of Guerin carcinoma.

Animals group	Growth factor φ, day^{-1}	Braking ratio κ, relative units
1 Control (without treatment)	0.252 ± 0.019	1.00
2 Conventional DOX	0.201 ± 0.017	1.25
3 DOX + EI	$0.183 \pm 0.004^{*}$	1.38
4 MNC	$0.185 \pm 0.006^{*}$	1.36
5 MNC + EI	$0.158 \pm 0.007^{*+}$	1.60

Notes: *Statistically significant difference from control group, $p < 0.05$. +Statistically significant difference from conventional DOX, $p < 0.05$.

RESULTS AND DISCUSSION

Changes in Nonlinear Growth Dynamics of Guerin Carcinoma After Magnetic Nanotherapy

The growth kinetics of animal tumors are shown in Table I. Conventional DOX treatment (group 1) resulted in minimal tumor response, while the combination therapy of MNC plus EI (group 5) had maximal antitumor effect. Treatment with DOX plus EI (group 3) and treatment with MNC alone (group 4) had intermediate antitumor effects. Our results show that the antitumor effect of MNC was increased when combined with EI. Tumors treated with MNC in the absence of EI (group 4) showed growth effects which were not significantly different from tumors treated with conventional DOX (group 2).

Magnetic Resonance Imaging

Figure 1 shows a representative image of a whole-body MRI scan of a rat with Guerin carcinoma 13 days after tumor transplantation. MNC was not administered, and so the Guerin carcinoma tumor without magnetic nanoparticles can be clearly seen. The heart, esophagus, lungs and other organs of the animal can be clearly distinguished.

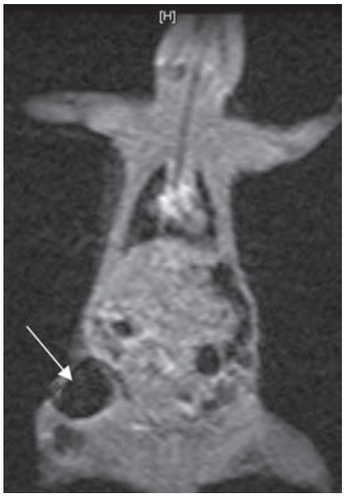

Figure 1. Whole-body MRI image of a rat with Guerin carcinoma in near hind leg. The rat belongs to the control group. The image was taken 13 days after tumor transplantation and no antitumor treatment was given. Arrow indicates tumor.

This allows evaluation of the overall health of the animals with transplanted tumors and exclusion of animals with an independent pathology.

Figure 2 shows MRI image of a rat with transplanted Guerin carcinoma that has undergone treatment with MNC in the absence of EI. Figure 2(a) shows the MRI image of the rat 13 days after tumor transplantation and before treatment. Figure 2(b) shows the same rat at 13 days post-tumor transplantation and 15 min after injection with MNC directly into the tumor. Figure 2(c) shows an MRI image of the same animal 8 days after treatment (21 days post-transplantation). The deformation left by the needle in the tumor after MNC injection can be clearly seen in Figure 2(b). Conglomerates of MNC are also clearly visible along the needle mark.

Figure 3 shows representative MRI images of a rat with Guerin carcinoma after treatment with both MNC and EI at 13 days post-tumor transplantation. Figure 3(a) shows an image of the carcinoma 2 hours after injection of MNC. Figure 3(b) depicts the same area after 15 min of EI. Table II shows the amount of diffusion of MNC that occurred as measured from these images. From the analysis of the MRI images, it can be seen that the position of MNC in the tumor did not change after local EI.

Ultrasound Imaging

B-Mode Sonography

Figure 4 shows the dynamics of changing B-mode US images during treatment of Guerin carcinoma with MNC and EI. Visual analysis of US images showed two areas where the tumor volume was more than 1 cm^3. Dark areas (hypoechogenicity) and bright areas (hyperechogenicity) can be interpreted as areas with low and high blood perfusion, respectively. While needle marks after treatment injection were visible in MRI pictures, such needle marks were only observable in US images after treatment with EI. We attribute this to increased echogenicity throughout the tumor, which is characteristic of the increase in blood perfusion.[17] After EI of the tumor, the nanoparticles conglomerates were visualized more clearly. In images taken from animals treated with both MNC and EI, nanoparticle conglomerates were observed after EI as points of hyperechogenicity in the tumor. This increased "point" echogenicity was observed 2–3 days after treatment. During palpation of tumors it was noted that after 3 session treatments, the density of animal tumors treated with MNC plus EI was significantly higher than that of control animals. In addition, high heterogeneity of the tumor was observed in animals treated with DOX plus EI (group 3) as well as animals treated with MNC plus EI (group 4) after 2 cycles of treatment.

Figure 5 presents changes in spatial autocorrelation in US images of Guerin's carcinoma after EI treatment. In general, the heterogeneity of tumor tissue with MNC or without MNC increased after EI (autocorrelation

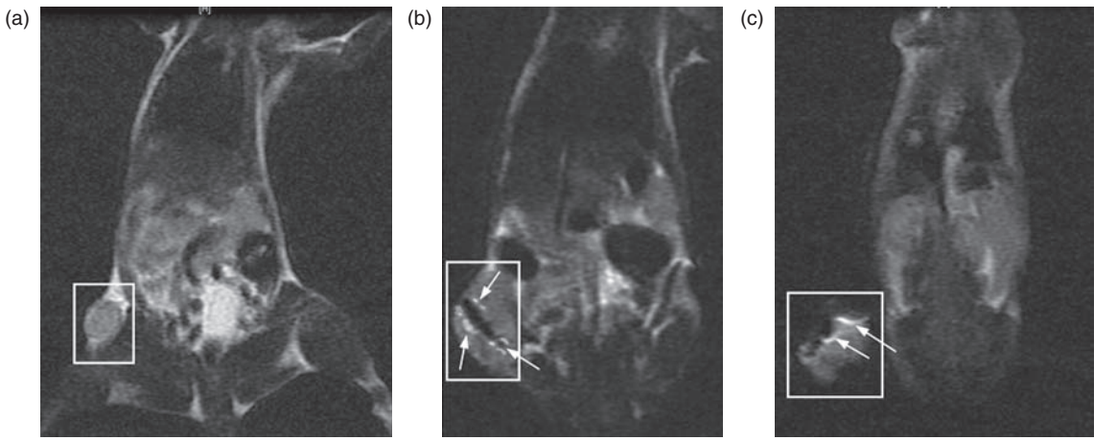

Figure 2. **MRI images of a representative Guerin carcinoma: (a) Control, 13 days after tumor transplantation, no treatment; (b) 15 min after treatment by MNC, 13 days after tumor transplantation; (c) 8 days after treatment with MNC (21 days after tumor transplantation). Arrows indicate the presence of MNC.**

decreased) as a result of intensification of blood flow.[18]

Doppler Ultrasound

Typical color Doppler US images of Guerin's carcinoma demonstrate a decrease of tumor blood vessel area after cancer treatment (Fig. 6 and Table III). The greatest decrease in vessel area was seen with MNC plus EI treatment (group 5), followed by MNC treatment alone (group 4), DOX plus EI (group 3), DOX alone (group 2) and control. These results provide confirmation that the treatment with maximal anti-angiogenesis effect consists of treatment with MNC plus EI.

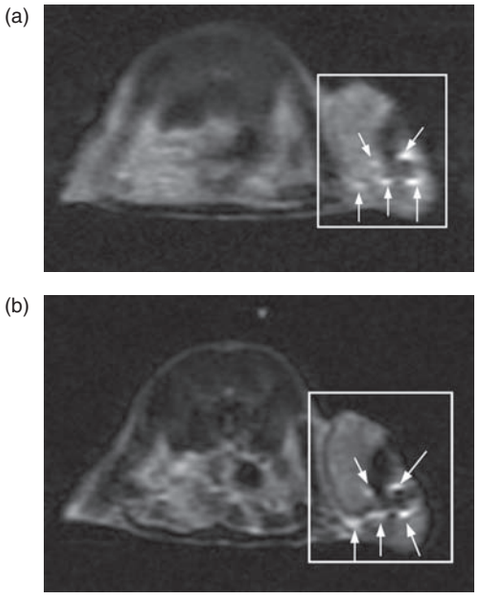

Figure 3. **MRI images of a representative Guerin carcinoma 13 days after transplantation. (a) 2 h after injection of MNC directly into the tumor and (b) after 15 min of EI. Arrows indicate the presence of MNC.**

Table II. **Comparison MNC diffusion in Guerin carcinoma under the influence of EI from MR images in Figure 3.**

	Disposition of MNC in tumor (arb-units)	
Section in tumor	Before EI	After EI
Normalized mean Radius (r.u.)		
Figure 3(a)	0.25 ± 0.07	0.23 ± 0.08
Figure 3(b)	0.16 ± 0.06	0.18 ± 0.08

Elastography and Dynamic Viscosity

In order to verify the observed trends in the antitumor effects of MNC and EI, we conducted elastography measurements of Guerin carcinoma during the second treatment session. We did not include animals treated with MNC alone (group 4) in these elastography measurements because we had already observed in the first treatment session that MNC alone had a weak antitumor effect (Table I). Figure 7 depicts the characteristic distribution of the Young's modulus for Guerin's carcinoma during treatment.

Qualitative analysis of these elastography images (Fig. 7) showed that the maximum difference observed was between the animals treated with MNC plus EI (group 5) and the other groups of animals. Quantitative analysis of US elastography in tumors (Table IV) during treatment showed a reduction of Young's modulus after treatment with DOX plus EI (group 3), but increased values for animals treated with MNC plus EI (group 5). The reduction after treatment with DOX plus EI is apparently related to the well-known fact that EI enhances blood perfusion through tumors.[17] The increase in Young's modulus seen

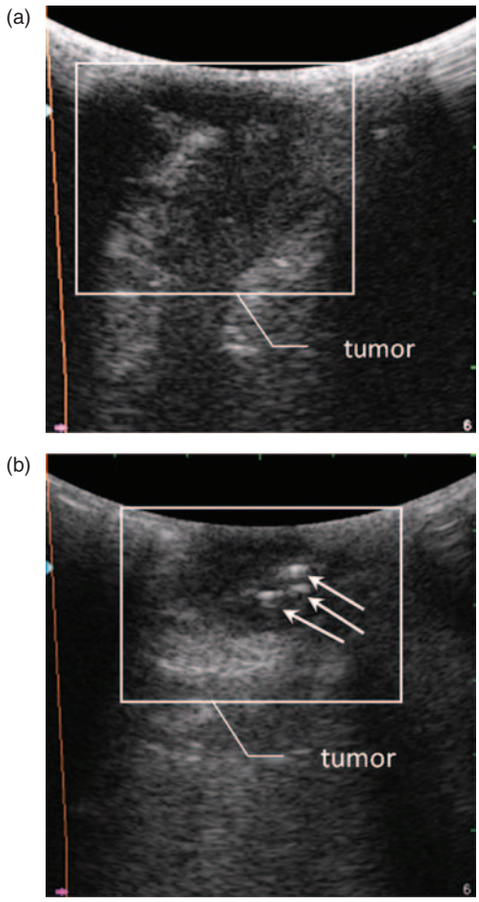

Figure 4. Dynamics of changing US images during treatment of Guerin carcinoma. Animal was treated with MNC plus EI 11 days after tumor transplantation (group 5). (a) 2 h after injection of MNC directly into the tumor and (b) after 15 min of EI. Arrows indicate the presence of MNC.

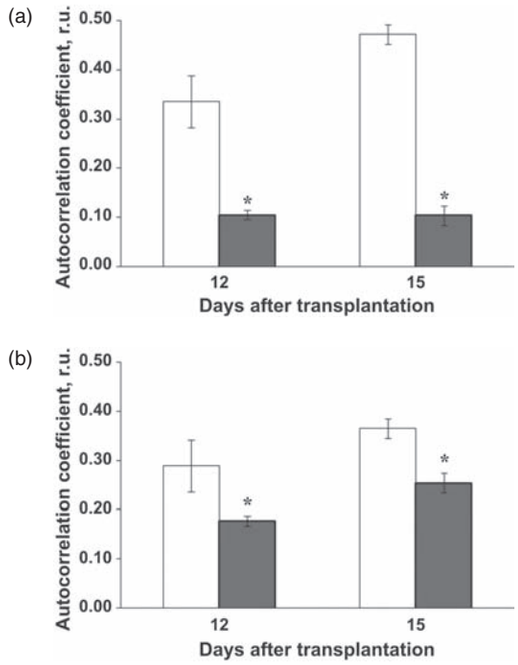

Figure 5. Change of spatial autocorrelation in EI-treated Guerin's carcinoma. (a) Animals treated with DOX plus EI but without MNC (group 3). (b) Animals treated with MNC plus EI (group 5). □—before EI; ■—after EI.
***Note*: * Statistically significant difference from before EI, $p < 0.05$.**

after MNC plus EI treatment may be due to the introduction of Fe_3O_4 nanoparticles.

Figure 8 shows elastography images depicting the distribution of the Young's modulus and viscosity for Guerin's carcinoma from an animal treated with MNC plus EI. The images were taken 21 days after tumor transplantation and 8 days after end treatment. Table V gives the calculated parameters of the Young's modulus for Guerin's carcinoma from different treatment groups 8 days after end treatment. E_{max}, the maximum value of the Young's modulus, and E_{av}, the average value of the Young's modulus, were increased in tumors treated with DOX plus EI (group 3), MNC alone (group 4) and MNC plus EI (group 5) compared to controls. σ_E, the standard deviation of the Young's modulus, and Ω entropy of the probability density function of the Young's modulus, were both increased in tumor treated with MNC plus EI (group 5) compared to controls. E_{max} was increased in tumors treated with MNC or MNC plus EI (groups 4 and 5) compared to tumors treated with DOX alone. Ω, was significantly increased in tumors treated with MNC plus EI (group 5) compared to tumors treated with DOX alone (group 2).

Figure 9 shows typical image histograms of the probability density elastic modulus for Guerin carcinomas 21 days after transplantation. Analysis of the histograms demonstrates that tumors from animals treated with MNC or MNC plus EI (groups 4 and 5) have more polymodal distributions than other tumors. The frequency distribution is characterized by more localized elasticity modes for tumor with nanoparticles, each having a higher frequency of occurrence than tissue tumors without MNC.

Quantitative analysis shows that the average parameter of dynamic viscosity (η_{av}) increased in tumors after treatment. (Table VI). This tendency is consistent with the observed changes of the Young's modulus of Guerin's carcinoma (Table IV) and vessel area in Doppler US image Guerin's carcinoma (Fig. 6, Table III).

DISCUSSION

Magnetic Nanotherapy of Tumors

We have recently reported that the combination of MNC plus EI was found to induce greater antitumor effect on Guerin's carcinoma than conventional DOX treatment.[9] Under our conditions, EI induces mild hyperthermia below 40 °C. Similarly we have reported that the combination of MNC plus EI was found to induce a

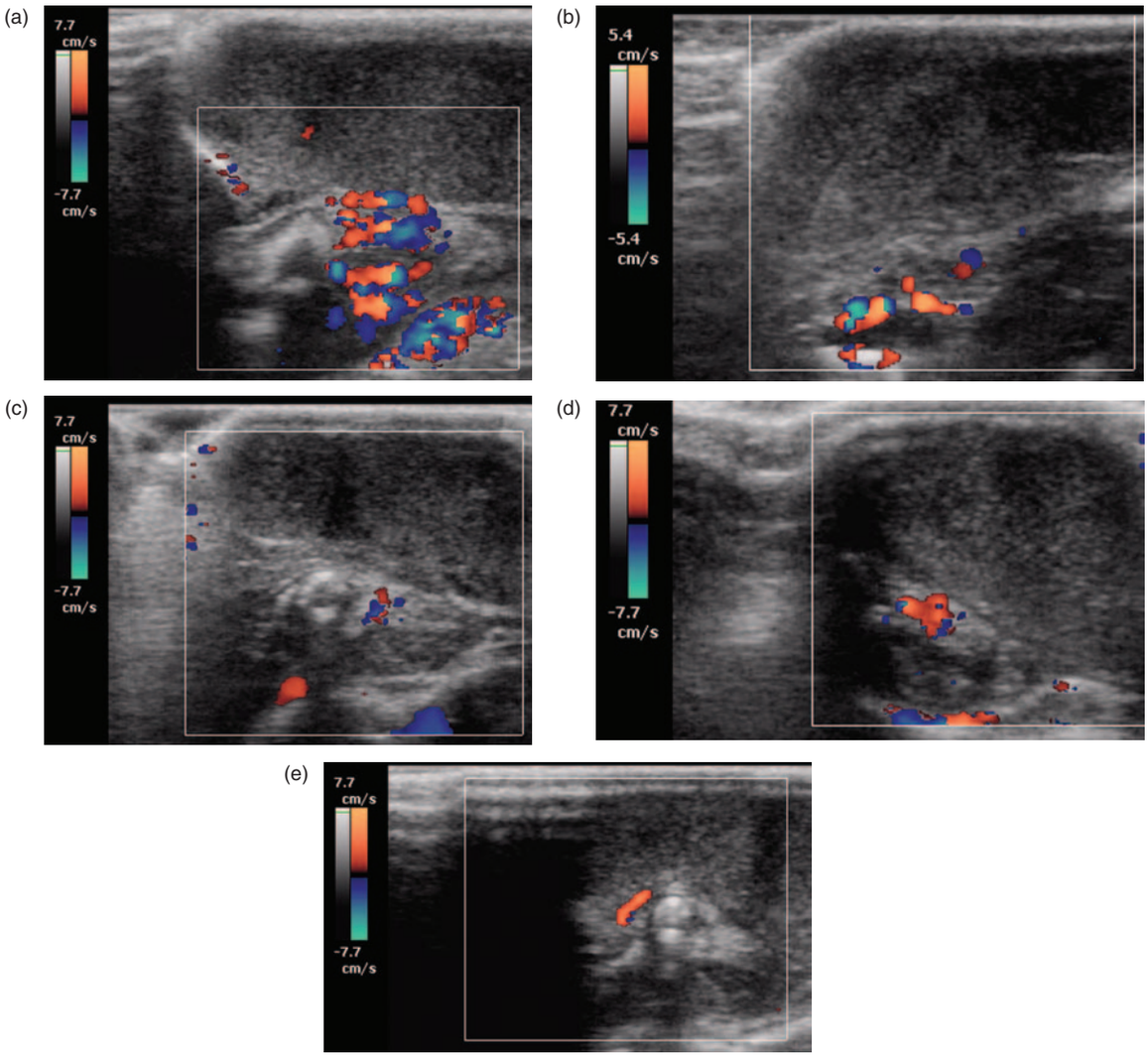

Figure 6. **Typical color Doppler US images of Guerin's carcinoma on 21 day after tumor transplantation and 8 days after the end of treatment. (a) Control, no treatment (group 1). (b) Conventional DOX treatment (group 2). (c) DOX plus EI (group 3). (d) MNC alone (group 4) (3). MNC plus EI (group 5).**

greater antitumor effect on Lewis lung carcinoma, which originates spontaneously as a carcinoma of the lung in C57BL mice.[19] In the latter study we discuss in detail the properties of the nanocomplexes and propose a mechanism to explain the observed effect. We briefly consider here our current results in the context of that prior evidence.

What is the relationships between the physicochemical reactions that occur during this treatment and the antitumor effects? It is possible to assume that the antitumor effects of our nanocomplexes increase due to the phenomenon of spin-dependent electron transport during EI between iron oxide and DOX aromatic rings and lactose hexose rings included with the anthracycline antibiotic as an ingredient. This is due to the fact that during magneto-mechanochemical synthesis, free radicals and electric charges are generated in large quantities in the nanoparticles as a result of the continuous collisions of working balls with the milling chamber wall. Long-lived free radicals are redistributed on the surface of DOX and magnetite

Table III. **The change of blood flow in typical color Doppler US images Guerin's carcinoma.**

	Animal group				
Parameter	1 Control (no treatment)	2 DOX	3 DOX + EI	4 MNC	5 MNC + EI
Vessel area (arb-units)	Over 10000	2600	2300	1700	500
S, cm/s	42.6	27.8	46.8	20.9	31.6
D, cm/s	14.0	12.9	22.3	11.8	18.5
S/*D*	3.0	2.2	2.1	1.8	1.7
RI	0.67	0.54	0.53	0.44	0.41

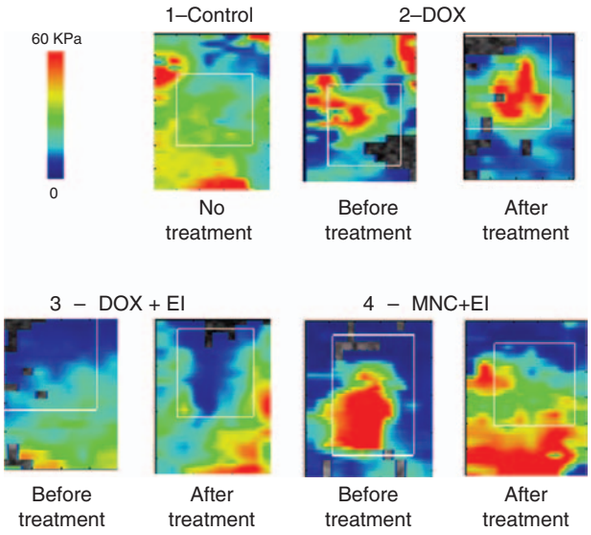

Figure 7. Typical elastography images (Young's modulus) of Guerin's carcinoma animal during second session treatment.

nanoparticles under the influence of the electromagnetic field. The magnetic properties of the complex particles are changed during magneto-mechano-chemical synthesis, in addition to a redistribution of electric charges and initiation of free radicals. This increased oxidative stress may lead to inhibition of mitochondrial electron transport and oxidative phosphorylation after treatment with MNC and EI. These processes are also known to cause inhibition of ATP synthesis in mitochondria of tumor cells, and to damage components of the cell. Furthermore, some reactive oxidative species act as cellular messengers in redox signaling pathways that induce apoptosis, necrosis and tumor cell death.[20]

Magnetic Resonance Imaging

We were able to use MRI to visualize MNC within tumors. This technique also allowed us to demonstrate that MNC retain their positions within the tumor after injection and do not diffuse under subsequent local EI for at least 2 hours after injection. This suggests the possibility of long-term fixed spatial arrangement of MNC in tumors and the possibility of using them to improve the accuracy of radiation treatment via irradiation with "Magnetotherm" (Radmir) using MNC as fixed coordinate in the tumors. This could lead to better outcomes during clinical use as it would minimize side effects in normal tissue.

It should be noted that the nanoparticles were non-uniformly dispersed in the tumors. This may partially impede the diffusion of drugs in some tumor cells. Therefore, better methods to improve the distribution of drugs into tumors, such as perhaps using multiple needles in different areas of a tumor, may be required.

Table IV. Calculated parameters of the Young's modulus for Guerin's carcinoma during 2-nd session treatment.

		Animal group, M ± m					
		2 DOX		3 DOX + EI		5 MNC + EI	
Parameter	1 Control (no treatment)	Before treatment	After treatment DOX	Before treatment	After treatment DOX + EI	Before treatment	After treatment MNC + EI
E_{av}, kPa	45.30 ± 22.70	36.63 ± 7.33	42.94 ± 5.22	29.96 ± 2.56	29.51 ± 2.49	52.86 ± 22.26	51.45 ± 12.58
σ_E, kPa	25.74 ± 12.67	25.48 ± 6.01	31.31 ± 4.71	22.03 ± 2.65	23.76 ± 1.41	35.64 ± 13.91	36.02 ± 11.50
Ω	3.60 ± 0.36	3.53 ± 0.11	3.73 ± 0.09	3.34 ± 0.04	3.25 ± 0.02*	3.70 ± 0.14+	3.78 ± 0.07+

Notes: *Statistically significant difference from before treatment 3 group; +Statistically significant difference from 3 group.

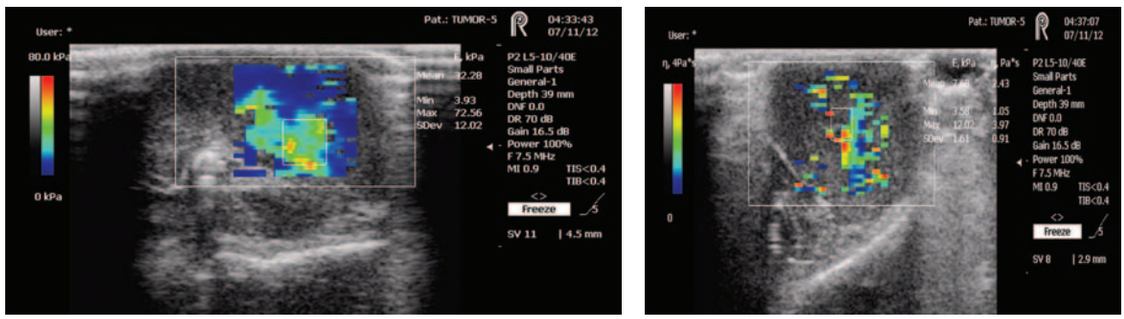

(a) (b)

Figure 8. Elastography images of Guerin's carcinoma in an animal treated with MNC plus EI (group 5). Animal is shown 21 days after tumor transplantation and 8 days after the end of treatment. (a) Distribution of the Young's modulus and (b) distribution of viscosity.

Table V. Calculated parameters of the Young's modulus for Guerin's carcinoma on the 21st day after transplantation of tumor and on the 8th day after the end treatment.

	Animal group				
Parameter	1 Control (no treatment)	2 DOX	3 DOX + EI	4 MNC	5 MNC + EI
E_{max}, kPa	54.90 ± 4.88	54.90 ± 5.43	58.14 ± 0.18*	69.80 ± 0, 66*,+	65.88 ± 6.87*,+
E_{av}, kPa	38.28 ± 9.27	42.76 ± 5.90	48.26 ± 6.56*	45.33 ± 2.12*	50.14 ± 10.05*
σ_E, kPa	27.75 ± 9.39	32.45 ± 8.04	37.67 ± 2.49	32.94 ± 1.78	39.71 ± 8.26*
Ω	3.20 ± 0.16	3.29 ± 0.16	3.42 ± 0.01*	3.34 ± 0.04	3.44 ± 0.16*,+

Notes: *Statistically significant difference from 1 group; +Statistically significant difference from 2 group.

It is well known that the magnetic field can affect the outcome of a biochemical reaction. The magnetic field is thought to influence the spin dynamics in the radical pair and thereby to determine the branching ratio between singlet states with antiparallel electron spins (↓↑) and triplet forms in which the electron spins are parallel (↑↑). Singlet-triplet transitions $S \leftrightarrows T$, which are usually forbidden by Wigner rule, allow transformation of a radical pair into the most reactive singlet state. The field due to a magnetic nanostructure may vary significantly over the extent of a single radical pair, causing the two spins to precess at different rates and about different axes. Relative reorientation of two spins leads to intersystem crossing.[21] An applied magnetic field causes these coherences to oscillate, leading to coherent interconversion of singlet and triplet electronic states of the radical pair and hence changes in the yields of recombination products and of free radicals in MNC within a tumor. The effect of the field may lead to extended lifetime of the relevant free radicals, and thus increase the therapeutic effect of the DOX in the MNC. On this basis we propose that magneto-mechano-chemical synthesis of MNC can be used not only to increase the sensitivity of MRI detection of various pathological processes, but also for use in simultaneous magnetic nanotherapy of cancer (theranostics).[22]

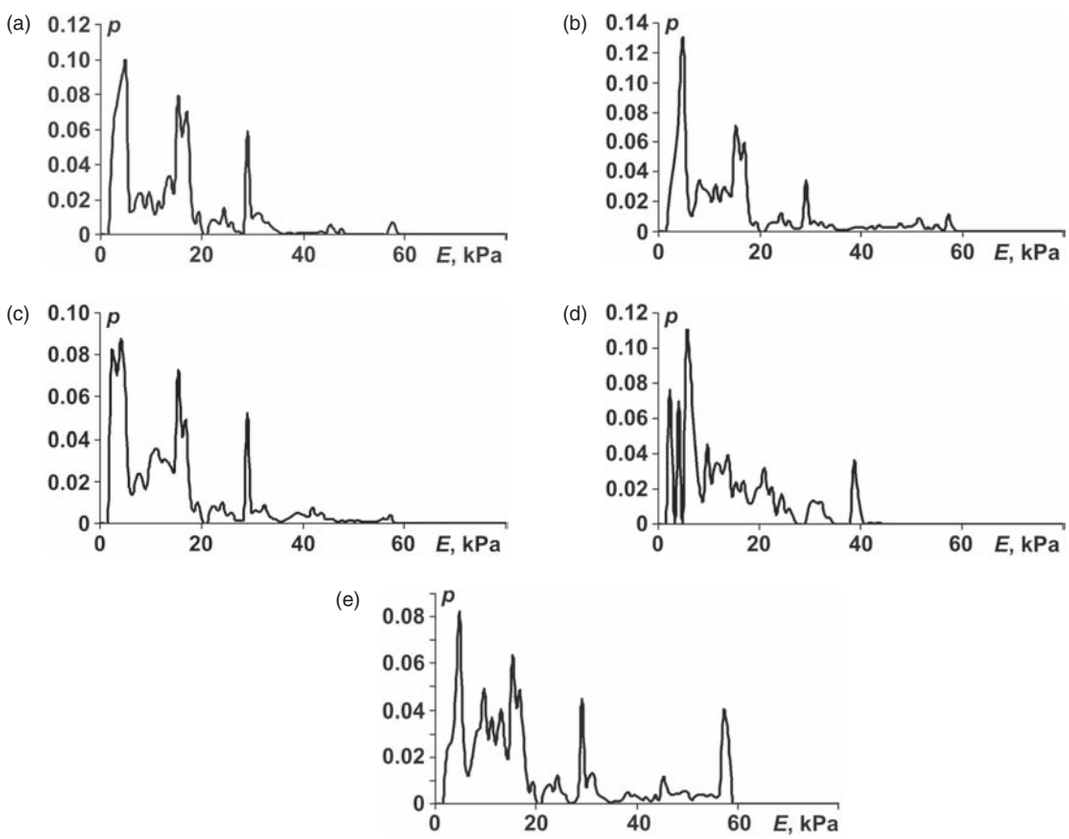

Figure 9. Typical histograms of the probability density elastic modulus of Guerin carcinomas 21 days after tumor transplantation and 8 days after the end of treatment. (a) Control, no treatment (group 1). (b) Conventional DOX treatment (group 2). (c) DOX plus EI (group 3). (d) MNC alone (group 4). (e) MNC plus EI (group 5).

Table VI. Typical calculated parameters of dynamic viscosity for Guerin's carcinoma on the 21st day after transplantation of tumor and the 8th day after the end of treatment.

	Animal group				
Parameter	1 Control (no treatment)	2 DOX	3 DOX + EI	4 MNC	5 MNC + EI
η_{av}, Pa·s	1.13	1.93	1.75	2.30	2.33

Ultrasound Imaging

Quantitative texture analysis of US images of Guerin's carcinoma demonstrated that the change in tumor heterogeneity seen after treatment exhibits nonlinear dynamics. Increased tumor heterogeneity was observed immediately after EI (decreased autocorrelation) at different stages of tumor treatment. The degree of change depended on the initial degree of blood perfusion.[18]

Color Doppler US imaging of Guerin's carcinoma after treatment indicated that maximal anti-angiogenesis effects were provided by the combination of MNC plus EI. This finding is encouraging for the outcome of future clinical trials, because the observable anti-angiogenesis effect may limit the haematogenous spread of metastases caused by the increase of blood perfusion during EI.[11,17] The reduction of blood flow and heterogeneity seen in the colour Doppler US images of tumors under EI, together with well-known effects of spatial chaos in MR imaging for malignant tumors, may be used as parameters in computerised medical diagnostics. Therefore, MNC is very promising as a contrast agent for the detection of metastases in cancer patients using US and MRI.

The present study revealed the dependence of displacement magnitude and strain relaxation not only on blood perfusion, but also on the tissue elasticity of Guerin carcinoma. The maximum value of the Young's modulus and of dynamic viscosity of tumors increased with MNC plus EI treatment compared with tumors in the untreated control group. The increase of the Young modulus may be indicative of cellular defects in tumor cell mechanotransduction. Such a defect may lead to initiation of apoptosis and necrosis in the tumor.[23]

CONCLUSION

In previous pilot experiments[9] and in this study of animals with transplanted Guerin carcinoma, we have shown that combination treatment with magnetic nanocomplexes based on Fe_3O_4 nanoparticles conjugated with doxorubicin plus subsequent local EI had a greater antitumor effect than treatment with conventional doxorubicin or treatment with magnetic nanocomplexe without EI. Analysis of MRI images showed that application of local EI did not affect the position of MNC in the tumor. B-mode sonography demonstrated that injection of MNC in the tumor and subsequent EI resulted in increased echogenicity throughout the tumor, which is characteristic of increased blood perfusion. Color Doppler US imaging shows that the largest decreases of vessel area in Guerin's carcinoma occurred after injection of MNC in the tumor and local EI. Elastography performed on a diagnostic ultrasound system showed that injection of MNC in the tumor increased Young's modulus for Guerin's carcinoma compared to the group of animals treated without nanoparticles.

In summary, our study demonstrates how MNC can combine imaging, diagnosis and therapy, such as chemotherapy, radiation therapy and hyperthermia, and be employed as nano-theranostic agents during US and MRI.[24]

REFERENCES

1. M. M. Shenoi, N. B. Shah, R. J. Griffin, G. M. Vercellotti, and J. Bischof, Nanoparticle pre-conditioning for enhanced thermal therapies in cancer. *Nanomedicine (Lond)* 6, 545 **(2011)**.
2. M. M. Amiji, Nanotechnology for Cancer Therapy, CRC Press, Boca Raton **(2007)**.
3. V. E. Orel, N. A. Nikolov, I. I. Dzyatkovska, O. Yu. Iaroshenko, A. V. Makarenko, A. L. Kaminska, M. N. Tkachenko, and I. B. Schepotin, Localization and scintigraphy vizualization of nanocomposite based on ^{99m}Tc-phosphate with Fe_3O_4 and KCl under radiofrequency hyperthermia on animal tumor Walker-256. *Reports National Acad. Sci. Ukraine* 10, 152 **(2011)**.
4. Magnetic resonance in Medicine, The basic textbook of the European Magnetic Resonance Forum, 4th edn., edited by P. A. Rinck, Blackwell Science, Berlin, Germany **(2001)**.
5. B. Kateb, K. Chiu, K. L. Black, V. Yamamoto, B. Khalsa, J. Y. Ljubimova, H. Ding, R. Patil, J. A. Portilla-Arias, M. Modo, D. F. Moore, K. Farahani, M. S. Okun, N. Prakash, J. Neman, D. Ahdoot, W. Grundfest, S. Nikzad, and J. D. Heiss, Nanoplatforms for constructing new approaches to cancer treatment, imaging, and drug delivery: What should be the policy? *Neuroimage* 54, S106 **(2011)**.
6. N. J. Hangiandreou, B-mode US: basic concepts and new technology. *RadioGraphics* 23, 1019 **(2003)**.
7. M. L. Palmeri, M. H. Wang, J. J. Dahl, K. D. Frinkley, and K. R. Nightingale, Quantifying hepatic shear modulus *in vivo* using acoustic radiation force. *Ultrasound in Med. Biol.* 34, 546 **(2008)**.
8. G. F. Pinton and G. E. Trahey, Sources of image degradation in fundamental and harmonic ultrasound imaging: A nonlinear, full-wave, simulation study. *Dahl. JJIEEE Trans. Ultrason. Ferroelectr. Freq. Control.* 58, 1272 **(2011)**.
9. V. Orel, T. Mitrelias, A.Shevchenko, A. Romanov, C. Barnes, M.Tselepi, A. Burlaka, S. Lukin, and I. Schepotin. Studies of complex magnetic nanoparticles with anticancer agents for cancer therapy. *J. Basic Appl. Phys.* 2, 8 **(2013)**.
10. V. E. Orel, A. D. Shevchenko, Yu. G. Mel'nik, N. A. Nikolov, I. I. Dzyatkovska, A. V. Romanov, A. P. Burlaka, S. M. Lukin, V. N. Uvarov, and I. B. Schepotin, Physicochemical characteristics of magnetosensitive nanocomplex obtained by mehanomagnetochemical technology of dry synthesis. *Metallofiz. Noveishie Tekhnol.* 32, 1157 **(2010)**.
11. V. E. Orel and A. V. Romanov, The effect of spatially inhomogeneous electromagnetic field and local inductive hyperthermia on nonlinear dynamics of the growth for transplanted animal tumors, Nonlinear Dynamics, edited by T. Evans, INTECH, Chroatia **(2010)**, pp. 285–308.
12. N. Nikolov, V. Orel; I. Smolanka, N. Dzyatkovskaya, A. Romanov, Y. Mel'nik, M. Y. Klimanov, and V. O. Chernish, Apparatus for Short-Wave Inductothermy "Magnetotherm," Proceedings of NBC 2008, edited by A. Katushev, Yu. Dekhtyar, and J. Spigulis, Springer-Verlag, Berlin, Heidelberg **(2008)**, pp. 294–298.

13. S. Girnyk, A. Barannik, E. Barannik, V. Tovstiak, A. Marusenko, and V. Volokhov, The estimation of elasticity and viscosity of soft tissues *in vitro* using the data of remote acoustic palpation, *Ultrasound Med. Biol.* 32, 211 **(2006)**.

14. N. Emanuel, Kinetics of experimental tumor processes, Nauka, Moscow **(1977)**, (In Russian).

15. G. A. Korn and T. M. Korn, Mathematical Handbook for Scientists and Engineers, MacGraw-Hill, New York **(1968)**.

16. H. Li, C. A. Calder, and N. Cressie, Beyond Moran's I: Testing for Spatial Dependence Based on the Spatial Autoregressive Model. *Geographical Analysis* 39, 357 **(2007)**.

17. V. E. Orel, T. S. Golovko, I. I. Smolanka, A. S. Krahmalova, and N. A. Nikolov, Ultrasonic visualization of intratumoral blood flow increase in patients with breast cancer under the influence of local radiofrequency hyperthermia, Radiation Diagnostics. *Radiation Therapy* N1, 43 **(2011)**, (In Ukrainian).

18. V. E. Orel, N. N. Dzyatkovskaya, A. V. Romanov, and T. M. Kozarenko, The effect of electromagnetic field and local inductive hyperthermia on nonlinear dynamics of the growth of transplanted animal tumors. *Exp. Oncol.* 29, 156 **(2007)**.

19. V. Orel, A. Shevchenko, A. Romanov, M. Tselepi, T. Mitrelias, C. Barnes, A. Burlaka, S. Lukin, and I. Schepotin, Magnetic properties and antitumor effect of nanocomplexes of iron oxide and doxorubicin. *Nanomedicine: Nanotechnology, Biology and Medicine* **(2014)**, In preparation.

20. M. Valko, C. J. Rhodes, J. Moncol, M. Izakovic, and M. Mazur, Free radicals, metals and antioxidants in oxidative stress-induced cancer, *Chem-Biol. Inter.* 160, 1 **(2006)**.

21. A. E. Cohen, Nanomagnetic control of intersystem crossing. *J. Phys. Chem.* 113, 11084 **(2009)**.

22. S. Akhter, F. Ramazani, M. Z. Ahmad, J. Ahmad, I. Ahmad, Z. Rahman, S. Amin, and F. J. Ahmad. Theranostic metallic nanomedicine in oncology: New insights and concerns, Frontiers in Anti-Cancer Drug Discovery, edited by Atta-ur-Rahman and M. Iqbal Choudhary, Bentham Science Publishers, University of Karachi, Pakistan **(2014)**, Vol. 3, pp. 262–291.

23. K. Rennier and J. Y. Ji, Shear stress regulates expression of death-associated protein kinase in suppressing TNFα-induced endothelial apoptosis. *J. Cell Physiol.* 227, 2398 **(2012)**.

24. S. S. Kelkar and T. M. Reineke, Theranostics: Combining Imaging and Therapy. *Bioconjugate Chem.* 22, 1879 **(2011)**.